Supplementary Information

1. Figures

Force transducer characteristics

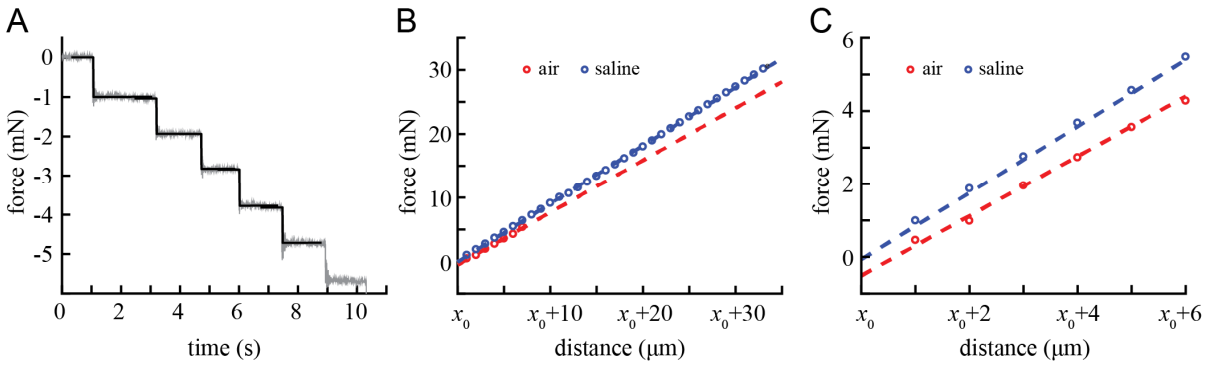

Fig S1. Linearity of the force transducer measurements. A) Raw data (grey) with superimposed fits (black) of two perpendicular razorblades pressed against each other. **B)** Force-deflection graphs for measurements in air (red) and saline (blue). The vertical offset between the curves is due to the difference in initial conditions (i.e. the vicinity of the razor blades before the step in which contact was made). **C)** First six deflection steps from the graphs shown in B. The dynamic range of the force transducer used in the experiments is 0–10 g, with a resolution of <1 mg (= 0.01 mN).

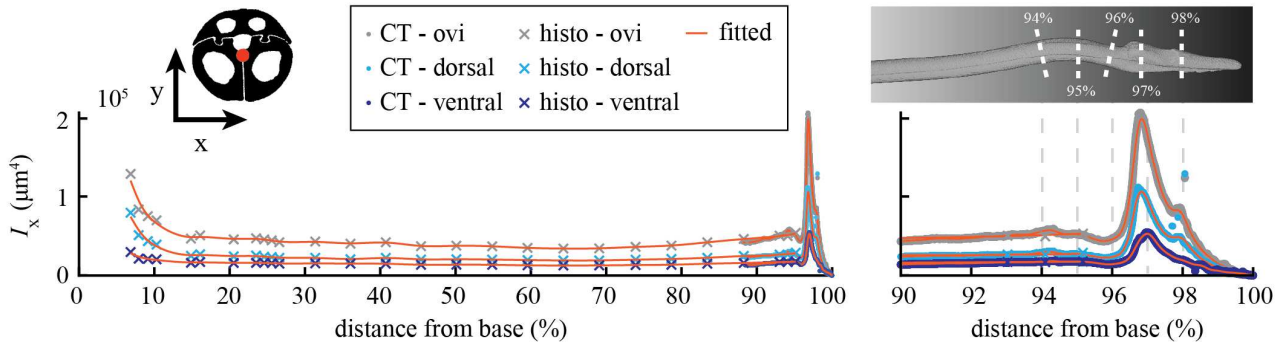

Fig S2. Contribution to the ovipositor second moment by individual valves. I_x values for the valves are higher than in **Fig 8A** because we used the centroid of the whole ovipositor (red dot in the schematics) in all calculations. The dorsal valve contributes more to the ovipositor second moment of area than each individual ventral valve, because compared to the ventral valves, a greater part of the dorsal valve is located further away from the ovipositor centroid.

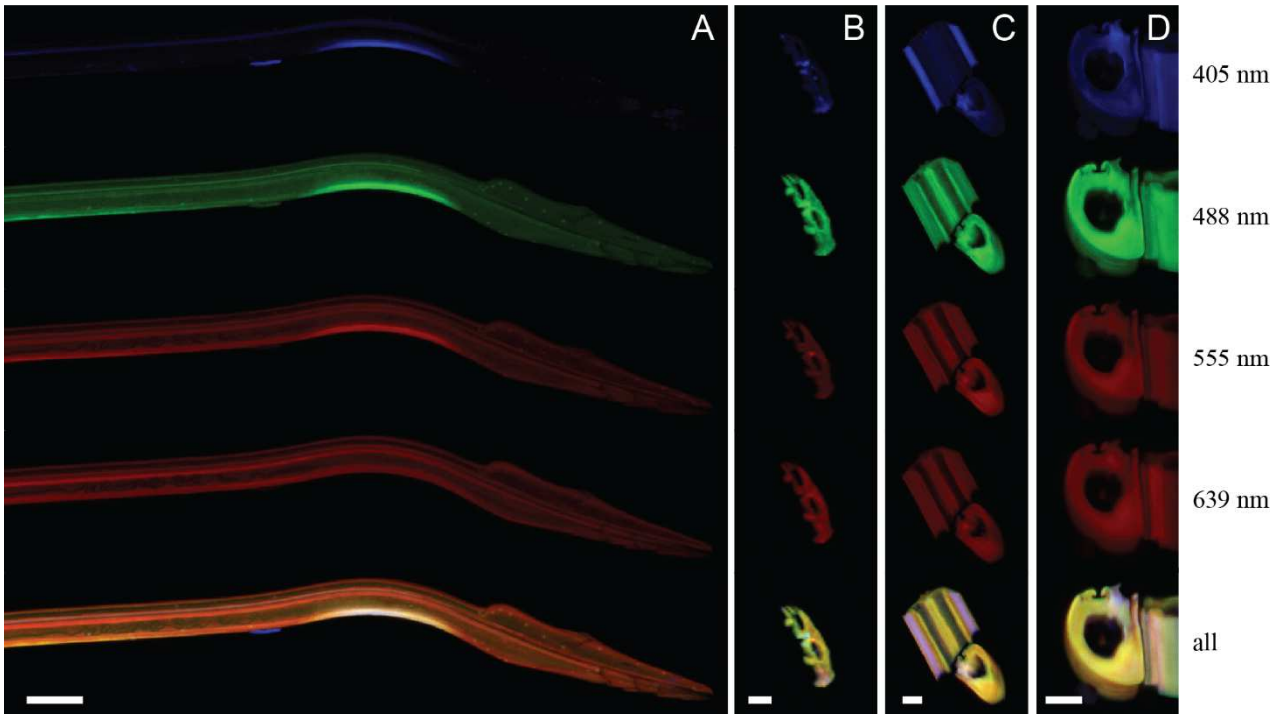

Fig S3. Autofluorescences (split in different channels) recorded from the ovipositor. Autofluorescence of materials excited with different wavelengths shows gradients in material composition in the distal part of the ovipositor. Excitation wavelengths indicated in the figure on the right. **A)** Distal part of the ovipositor. **B, C, D)** Sections from the distal region of the ovipositor, but proximal to its S-shaped region. (**B**) Dorsal valve cross-section (**C**) Dorsal valve inner side and ventral valve cross-section. The scan was optimized for the dorsal valve and the colours of the ventral valve might not be representative of its material composition. (**D**) Ventral valve cross section and side view. The scan was optimized for the cross-sectional view, so the colours of the side view do not reflect the material composition of the valve. Scale bars: 50 µm (**A**), 10 µm (**B–D**).

2. Tables

Table S1. Mean Second Moment of Area of regions of fitted data based on CT-scans only. For centroids see Fig 3. The shaft, S-region and tip are for each structure significantly different (Mann-Whitney *U* test, P<0.05). The bulge is defined as the part of the tip where I_x is larger than the mean I_x of the shaft.

	Second Moment of Area (I_x, µm^4 1 × 10^4)			
	Shaft <93% OL	S-Region 93-96% OL	Tip-region >96% OL	Bulge
Dorsal valve	0.25 ± 0.02 max=0.27 (n=1655)	0.30 ± 0.06 max=0.39 (n=999)	1.27 ± 1.05 max=3.06 (n=1227)	96.29–99.41 %OL Mean = 1.60 ± 0.97 (n=941)
Ventral valve	0.94 ± 0.10 max=1.13 (n=1555)	1.06 ± 0.10 max=1.16 (n=1001)	0.55 ± 0.54 max=1.61 (n=1229)	96.14–97.21 %OL Mean = 1.30 ± 0.22 (n=347)
Whole ovipositor	4.51 ± 0.28 max=5.04 (n=1665)	5.13 ± 0.39 max=5.74 (n=1018)	7.31 ± 5.78 Max=19.93 (n=1208)	95.99–98.34 %OL Mean = 10.21 ± 4.82 (n=769)

Table S2. Measured bending stiffness and calculated effective modulus of elasticity of the shaft and S-region of ovipositors, dorsal and ventral valves. Diff. indicates the significance level of the difference between the shaft and S-region for the specific parameter obtained with a Mann-Whitney *U* test. When comparing values within each column, only the E_{eff} of the shaft of the ventral valve and the whole ovipositor do not significantly differ (Mann-Whitney *U* test, P=N.S.).

	Bending stiffness ($E_{eff}I_x$, 1 × 10^{-11} Nm^2)				Effective modulus of elasticity (E_{eff}, GPa)		
	Shaft <93% OL	S-Region 93-96% OL	Diff.		Shaft <93% OL	S-Region 93-96% OL	Diff.
Dorsal valve	0.90 ± 0.33 (n=30)	0.88 ± 0.52 (n=10)	P=N.S.		5.95 ± 2.53 (n=30)	3.70 ± 2.51 (n=10)	P<0.01
Ventral valve	4.40 ± 1.85 (n=26)	1.57 ± 0.85 (n=10)	P<0.001	P=N.S.	4.81 ± 2.56 (n=26)	1.46 ± 0.74 (n=10)	P<0.001
Whole ovipositor	15.72 ± 5.37 (n=42)	5.12 ± 1.09 (n=11)	P<0.001		3.60 ± 1.27 (n=42)	0.92 ± 0.35 (n=11)	P<0.001

3. **Movies**

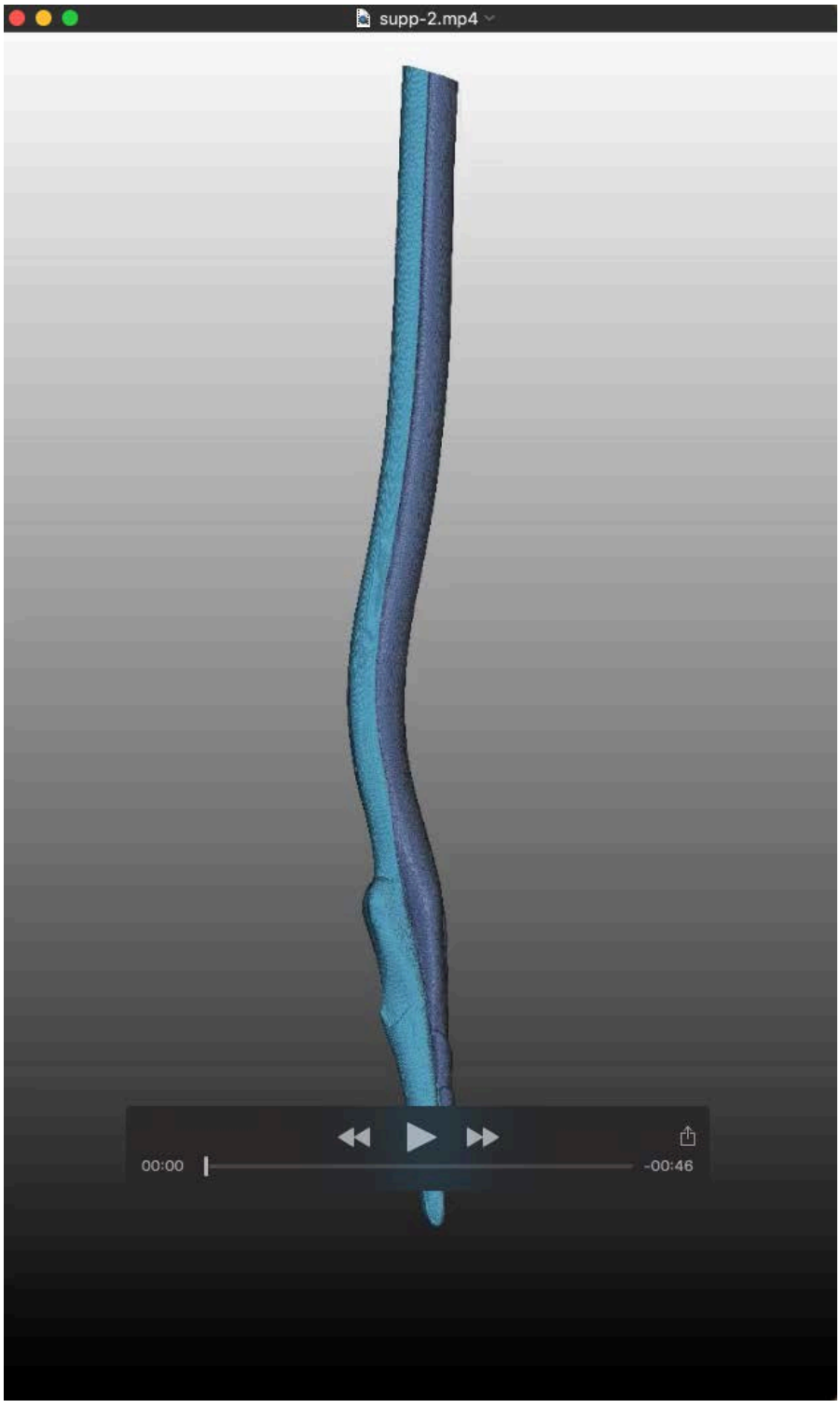

Movie 1. Segmented µCT scan of the ovipositor. Colour code same as in graphs (**Fig 3**); dorsal valve is light blue and ventral valves are dark blue. The characteristic S-shaped region of the ovipositor, the bevel shaped tips, the widening of the dorsal valve, and the serrations on the ventral valves are clearly visible. Additionally, tongue-and-groove mechanisms on the inner sides of the ovipositor are straight and do not show morphological variations.

Movie 2. Curved and straight ovipositor insertions in the substrate. Protraction of ventral valve(s) within the substrate leads to dorsal curving of the ovipositor's distal end. In contrast, protraction of the dorsal valve within the substrate does not lead to noticeable curving of the ovipositor, which therefore makes a straight path. Videos obtained as described in Cerkvenik et al. (2017). Videos show insertion in 2% gelatine, slowed down approximately 10x.

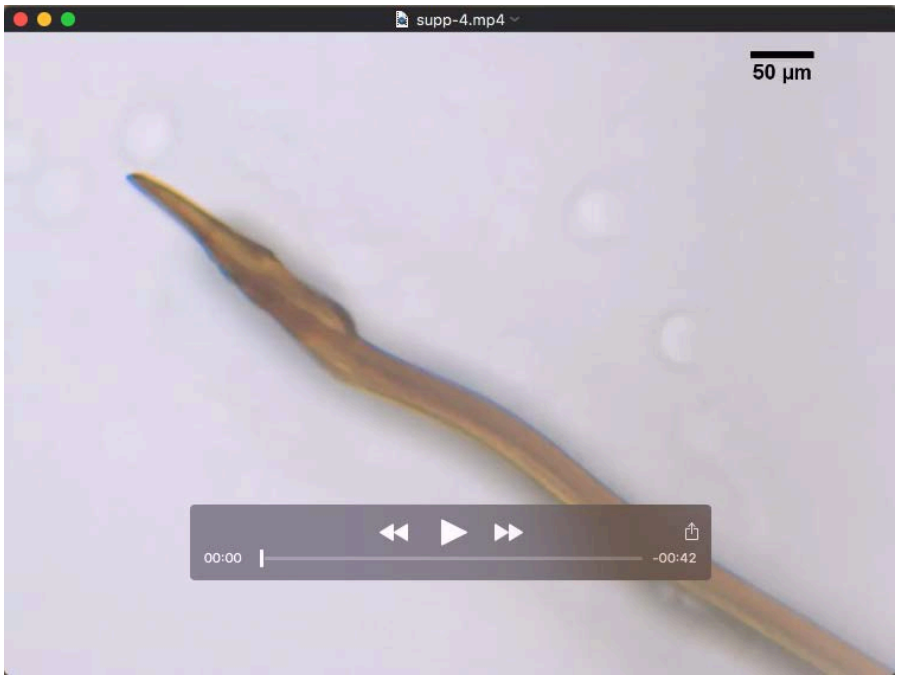

Movie 3. Valve movements outside the substrate. Spontaneous valve movements outside the substrate observed under microscope—the animal was **not** in the probing position and a cover glass was put on top of the ovipositor to keep it in the focal plane. Protraction of both the dorsal and the ventral valves causes dorsal curving of the ovipositor distal end. Video recorded with Leica DFC 450 C camera (5 MP) mounted on Leica DM6b microscope (Leica Microsystems). Slowed down approximately 4x.